Butterfly curves and critical modes for second-order spin-wave instability processes in yttrium iron garnet films

P. Kabos,[a] C. E. Patton, G. Wiese, A. D. Sullins, E. S. Wright, and L. Chen
Department of Physics, Colorado State University, Fort Collins, Colorado 80523

(Received 5 April 1996; accepted for publication 17 May 1996)

Combined Brillouin light-scattering (BLS) and microwave pumping techniques were used to measure the second-order spin-wave instability threshold microwave field amplitudes and characterize the critical modes for ferromagnetic resonance (FMR) saturation in 4.15 μm-thick yttrium iron garnet films at 8.47 GHz with the static magnetic field in-plane. To the best of our knowledge, this work represents the first BLS measurements for second-order FMR saturation processes in ferrite materials. Several new results were obtained: (1) A new type of butterfly curve for second-order processes. (2) Strong scattering from modes at low wave numbers in the 10^4 rad/cm range. (3) An observed in-plane propagation direction for these low wave number modes at 90° to the in-plane static field direction. These results differ significantly from the behavior expected from the bulk sample instability theories of Suhl and Schlömann, which predict critical modes at wave numbers and propagation directions in the 10^5–10^6 rad/cm and 0° ranges, respectively, and a sharp cusplike response centered at FMR. These results indicate that significant modifications of the bulk theory, which take into account the real modes supported by the film, are needed to realistically model second-order instability processes in films. © *1996 American Institute of Physics.* [S0021-8979(96)07916-9]

I. INTRODUCTION

Single-crystal yttrium iron garnet (YIG) thin films prepared by liquid phase epitaxy or pulsed laser deposition techniques are strong candidates for practical applications in planar microwave signal processing devices. The microwave response of such films as a function of the input power level is one important consideration for such devices. When the power is very low, typically in the mW range, one obtains a narrow ferromagnetic resonance (FMR) linewidth, absorption spectra which may include a variety of spin-wave resonance peaks, and the possibility of propagating magnetostatic waves which may be used for various applications such as delay lines, filters, and signal-to-noise enhancers. This linear response regime is well documented.[1,2]

The situation is different at increased power levels. A wide variety of nonlinear effects can be observed even at modest power levels, still in the mW range. Three basic effects have been studied to date: (1) FMR foldover effects,[3–8] (2) auto oscillations which may evolve into a chaotic microwave response under certain conditions,[9] (3) modifications in the below resonance response at high power levels under conditions which correspond to parallel pumping or subsidiary absorption responses connected with first-order instability processes.[10]

Critical to the fundamental understanding of the nonlinear effects listed above is a working knowledge of the critical spin-wave modes which are excited above thermal levels at the onset of the nonlinear behavior. A systematic determination of these critical modes has been made only for subsidiary absorption and parallel pumping. Such determinations were based on two approaches, one microwave and one optical. The microwave technique involved the measurement of the critical microwave field amplitude for the nonlinearity onset as a function of static field and theoretical fits to the data.[11–13] This yielded indirect information on the nature of the critical modes. The optical technique involved Brillouin light scattering (BLS) on the parametrically excited magnons above the nonlinear response threshold.[14–16] From BLS measurements, it was possible under certain conditions to identify the critical modes directly. In some cases, these identifications support the application of bulk theory for the nonlinear processes.[15] In others, new theories have been needed which take into account the special nature of the spin-wave modes in the thin-film geometry.[10,12,13]

To date, there have been no reports on the experimental identification of the critical modes which must accompany the nonlinear response effects at or near ferromagnetic resonance. Given the fundamental importance of nonlinear effects associated with FMR for the understanding of foldover and chaos, for example, and the technological importance of these same effects for YIG film microwave devices such as resonators and filters, such identifications would be extremely useful. The objective of this work was to apply microwave and BLS techniques to the nonlinear response at or near ferromagnetic resonance, identify the critical modes which participate in this response, and compare the experimental results with available theory.

The strategy was based on previous experience with both types of measurements for first-order processes and for low power FMR. In the case of microwave measurements, careful determinations of so-called butterfly curves of the threshold microwave field amplitude for instability as a function of static field, in combination with detailed theoretical fits, yielded quantitative but indirect information on the wave number k and propagation angle θ_k values versus field for

[a]Presently on leave of absence from the Faculty of Electrical Engineering and Information Technology of the Slovak Technical University, Bratislava; Electronic mail: kabos@lamar.colostate.edu

 0021-8979/96/80(7)/3962/10/$10.00 © 1996 American Institute of Physics

the critical modes.[10–13] In the case of BLS measurements applied to parallel pumping and subsidiary absorption, it was possible to make direct identifications of these critical mode k and θ_k values over the field ranges for which the modes could be accessed by light scattering. In the case of BLS measurements applied to FMR it was possible to detect the ferromagnetic resonance signal from the scattered magnons at zero wave number.[17]

The focus of this work was to apply BLS techniques to resonance saturation. The specific objectives were threefold: (1) To measure the threshold microwave powers and field amplitudes for the second-order instability onset at ferromagnetic resonance, and for a range of magnetic fields near the FMR field. (2) To use these threshold data to construct a new type of butterfly curve, one for second-order instability processes associated with resonance saturation, and use this curve to identify the relevant critical modes. (3) To use the BLS scattering geometry to identify, insofar as possible, the pumped magnon modes which are the source of the BLS signal.

From the discussion to follow, it will be evident that the range of accessible k values by the BLS technique, typically in the range of zero to 10^4–10^5 rad/cm, are well below the expected critical mode k values which are excited in high power FMR experiments. The initial expectation, then, was that the BLS technique would detect only relatively low wave number magnons associated with the pumped FMR response, and not the high k magnons excited parametrically. The actual results turned out to be quite different. The BLS data revealed low wave number critical modes and propagation angles for these modes which were not in accord with the bulk theories. The results indicate that the nonlinear processes which are responsible for resonance saturation in YIG films are quite different from those which are operative in bulk ferrite materials.

II. NONLINEAR SPIN-WAVE INSTABILITY PROCESSES

There are two different parametric processes which can affect the microwave response in general, and the FMR response in particular, at high power levels. Detailed discussions of these processes are contained in the classic reports of Suhl and Schlömann as well as several more recent reviews.[18–21] The material below is intended to provide a brief summary of these effects.

A. First-order processes

If the pump frequency ω_p is sufficiently low, it is possible to excite parametric spin waves at one half the pump frequency. In this case, the processes are termed ''first order'' or ''three magnon'' processes. Both terms derive from the formalisms of Suhl and Schlömann which have been notably successful in explaining many of the essential features. The term first order refers to the appearance of an FMR dynamic response amplitude term in the coupling expression to the first power. The term three magnon refers to the modes which are coupled, namely, *one* uniform mode magnon and *two* other magnons associated with oppositely propagating spin wave of nonzero wave vector.

First-order processes are allowed only if the sample can support such spin waves at one half the pump frequency. This condition is required to conserve energy as the uniform mode FMR magnon at ω_p converts into two spin-wave magnons at $\omega_k = \omega_p/2$. First-order processes for samples biased at ferromagnetic resonance are possible only at low frequencies because of this $\omega_k = \omega_p/2$ condition. For high-frequency FMR, typically above 4 GHz or so, depending on sample shape, the magnetization, etc., the magnetic field is relatively high and the spin-wave band limits are all above the $\omega_k = \omega_p/2$ point. In this situation, first-order processes are not supported. First-order processes may still be supported, however, if the magnetic field is well below the field required for FMR, such that the spin-wave band falls below the $\omega_k = \omega_p/2$ cutoff point. The observed absorption which occurs in this situation under high power conditions is termed ''subsidiary absorption'' because it occurs, typically, for fields well below the FMR field.

The above effects occur when the microwave field is applied perpendicular to the static field. Schlömann and coworkers discovered that similar effects could be induced when the microwave field was applied parallel to the static field.[22] Here, as for subsidiary absorption, one obtains a pronounced absorption over a range of fields well below the FMR field. The novel result, of course, is the occurrence of any absorption at all. In the linear response analysis, there is no coupling between the parallel pumping microwave field and the dynamic magnetization response of the sample.

The original first-order theories give specific predictions of the critical spin-wave modes which are parametrically excited in the subsidiary absorption and parallel pumping experiments. Critical modes at a propagation angle θ_k at 30°–40° relative to the static field, where allowed by the $\omega_k = \omega_p/2$ condition, are predicted for subsidiary absorption. Critical modes at $\theta_k = 90°$, where allowed, are predicted for parallel pumping. One by one, various additional effects have been uncovered which affect the nature of the critical modes for first-order processes. These include the effect of various pumping configurations and sample shape,[23,24] the effect of a wave vector dependent relaxation rate for the parametric modes,[11] and specific mode quantization effects for specific sample shapes.[12,13]

Historically, one particular type of measurement and calculation has formed the basis for most first-order instability measurements and calculations. This is the so-called ''butterfly curve'' which is a plot of the critical microwave field amplitude at the instability threshold as a function of the static magnetic field. Curves of this type may be found in many of the references cited above. The shapes of these curves give detailed information on (1) the critical mode wave vector **k** as a function of field and (2) the **k** dependence of the relaxation rate of these modes. On the whole, the theory for first-order instability processes is in good agreement with both microwave results and BLS determinations of the properties of the critical modes and these butterfly curves. A detailed review of these results is beyond the scope of this article. The interested reader is referred to the citations given above.

B. Second-order processes

The term ''second order'' derives from the form of the analytical coupling expressions under conditions when the first-order processes may be excluded from consider ation.[18,19] The next level coupling terms involve the square of the FMR response amplitude. Since the FMR response amplitude is typically small, first-order terms, where allowed, will be much larger than second-order terms. When first-order processes are not allowed, however, the nonlinear response threshold will be determined by these second-order coupling terms. Second-order processes are also referred to as ''four magnon'' processes. This terminology derives from terms in the corresponding Hamiltonian which contain *two* uniform mode magnon creation operators and *two* spin-wave magnon destruction operators. This means that two uniform mode magnons each at ω_p transform into two oppositely propagating spin-wave magnons each at ω_k. Energy conservation leads to the condition $\omega_k = \omega_p$. Second-order processes, therefore, involve parametric magnons at the same frequency as the pump frequency. For a typical magnetic sample excited at ferromagnetic resonance, one typically has some part of the spin-wave band degenerate with the FMR pump frequency. In general, this means that second-order processes will always be allowed for fields at or near the fields responsible for FMR.

As for first-order processes, the original theories of Suhl and Schlömann give specific predictions for the values of the wave number k and propagation angle θ_k for the modes with the lowest microwave power threshold and, hence, the critical modes which will be driven unstable first under given experimental conditions. The basic result here is that, where allowed, the modes with the lowest threshold will be at $\theta_k = 0°$. Under FMR conditions, critical modes at $\theta_k = 0°$ will correspond to k values in the 10^5–10^6 rad/cm range. The algebraic details of the analysis for second-order processes are much more involved than those for first-order processes. In spite of the importance of these effects to the understanding of microwave processes in ferrite materials in general and FMR at high power levels in particular, published theoretical results are essentially limited to the original articles of Suhl and Schlömann already cited. Recently, the work on first-order processes for different shapes and pumping configurations cited above[23] has been extended to second-order processes. Some of these results will be summarized in Sec. III. These results will serve as a basis for comparison with the available theory.

III. EXPERIMENT

The YIG film Brillouin light-scattering measurements followed the procedure described by Wilber and coworkers[14,15,25] and Kabos *et al.*[16] The sample for the measurements shown below was a 4 mm×4 mm, 4.15-μm-thick single-crystal YIG film grown by liquid phase epitaxy (LPE) on a gadolinium–gallium–garnet (GGG) substrate. The YIG films for this work were provided by Dr. J. D. Adam of the Westinghouse Science and Technology Center, Pittsburgh, Pennsylvania. LPE films are usually grown on both sides of the GGG substrate. The film on one side of the substrate was polished off to allow for unambiguous measurements on a single well defined film.

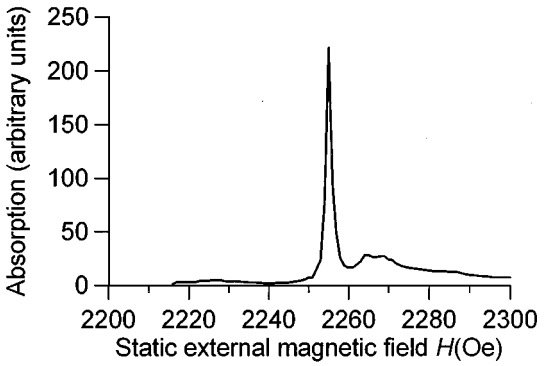

FIG. 1. Low power FMR resonance curve for the in-plane magnetized 4.15-μm-thick YIG film in the shorted waveguide system. The pump frequency was 8.47 GHz.

The first step in the experiment for a given film was to measure the usual low power FMR response of the sample. This was done with a modified Varian Model 4500 microwave spectrometer at 8.47 GHz. Due to strong cavity loading effects which occurred for the relatively large area, narrow linewidth single-crystal YIG films, these FMR profiles were obtained with the sample mounted close to the narrow sidewall of a waveguide short and at a position where the microwave magnetic field is maximum. The static magnetic field and the linearly polarized microwave field were both in the plane of the film and mutually orthogonal.

A typical FMR absorption curve is shown in Fig. 1. The curve shows a strong main FMR resonance line followed by a small shoulder response at higher fields. The half power linewidth for the main peak is 1.5 Oe, and is typical of high quality single-crystal YIG films. The somewhat broader loss peak on the high-field side of the main FMR line is due to the excitation of magnetostatic modes. These modes are particularly pronounced because of the relatively large size of the sample, relative to the one-half wavelength standing wave of the microwave field excitation at the sample position. As will be established shortly, this same pumping configuration was used for the BLS measurements, albeit in a waveguide cavity instead of a short. This magnetostatic mode shoulder will be one consideration in the BLS results. While it would have been useful to reduce this extra loss peak by using a smaller sample or positioning the film in a region with a more homogeneous microwave field, the constraints imposed by the BLS measurements made such modifications impractical.

Turn now to the main experimental system for this work, the combined cavity spectrometer and Brillouin light-scattering system. The experimental microwave/BLS setup is shown schematically in Fig. 2. The diagram shows: (1) A microwave cavity which contains the YIG film sample and an electromagnet to provide the in-plane static magnetic field. (2) Incident optics to focus the laser light on the sample. (3) Collection optics to obtain the scattered light signal for analysis by the Fabry-Pérot interferometer. Both

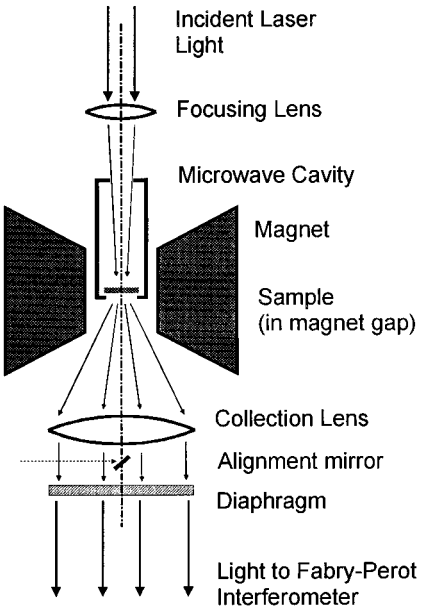

FIG. 2. Schematic diagram of microwave cavity, incident optics, and collection optics for the forward-scattering BLS detection of magnons, and the alignment mirror for use in a back scattering arrangement.

the film and cavity are shown in cross section. The collection optics arrangement includes a collection lens and a special diaphragm for wave vector selection. An additional mirror, just after the collection lens, is used to direct laser light on the sample in a backscattering geometry in order to focus and align the collection lens accurately.

The reflection microwave cavity was obtained by adding a coupling iris, not shown, to the waveguide short used for the FMR measurements. The sample position in the cavity was the same as before. A cavity rather than a short was needed to obtain a large enough microwave field amplitude at the sample to obtain nonlinear effects. The need for a cavity also resulted in significant loading effects at FMR, due to the narrow linewidth and extremely sharp FMR signal for the sample. These loading effects precluded any unique cavity calibration to obtain the microwave field amplitude at the sample as a function of input power. The threshold data to be presented shortly will be given in terms of input power to the system or in terms of relative power, as appropriate. It will be important to consider cavity loading effects in the interpretation of the data.

The applied external static magnetic field and the linearly polarized microwave field were both in the film plane and mutually perpendicular to achieve the desired in-plane field FMR configuration. The unloaded resonant frequency of the cavity was 8.47 GHz, the same frequency used for the shorted guide data shown in Fig. 1. With the sample in position, the cavity frequency shifted somewhat, and the FMR peak position in field shifted as well. Power was provided by a microwave sweep generator operated in a fixed frequency mode and amplified by a traveling wave tube (TWT) amplifier. Under typical measurement conditions, the field was set for some desired value and the microwave frequency was tuned manually to compensate for small changes in the cavity frequency due to sample loading. Such changes were small, typically in the 100 MHz range. The microwave power level was measured at the TWT amplifier output. The FMR peak occurred at a field of about 2300 Oe with a cavity frequency close to 8.60 GHz.

The optical system was similar to that described in the references cited above. The BLS measurements were made in the forward scattering configuration shown schematically in the Fig. 2 diagram. The single mode laser source was operated at a wavelength of 488 nm. Optical access was accomplished with small openings in the walls of the cavity. The scattered light at frequency $\omega_k = \omega_p$ was measured with a Sandercock type high contrast multipass tandem 3+3 Fabry-Pérot interferometer.[26] The spin-wave instability threshold power levels were determined from the onset of scattering, as will be discussed shortly.

The collection optics arrangement determines the range of critical mode wave vectors which can be detected in the forward scattering BLS arrangement shown in Fig. 2. First, the positioning and radius of the collection lens sets an upper limit on the magnitude of the in-plane of wave vector which can be detected. The 50 mm focal length, 1:1.4 collection lens used here corresponds to a wave number upper limit of about 4×10^4 rad/cm. Second, the backscattering alignment mirror blocks out the forward scattered light close to the optic axis and sets a lower limit on the accessible magnon wave numbers. This lower limit was about 100 rad/cm. This blocking mirror turned out to be a convenient feature for resonance saturation measurements, since the arrangement also serves to block the direct detection of the uniform mode FMR magnons at zero wave number.

The setup in Fig. 2 also provides for wave-vector selection. The diaphragm which follows the collection lens consists of a blocking plate with a narrow 200-μm-wide slit. By rotating this diaphragm about the optic axis, one can select out particular in-plane wave-vector directions. When the slit is parallel to the static magnetic field direction, or the horizontal direction in Fig. 2, one selects magnons with **k** vectors which are parallel to the field. When the slit is rotated 90°, or out of the plane of the page in Fig. 2, one selects magnon **k** vectors which are perpendicular to the field direction. For the actual measurements, one can determine the critical mode propagation angles by slowly rotating the slit diaphragm while monitoring the scattered light at $\omega_k = \omega_p$. Details on forward scattering techniques for the detection of magnons can be found in the references cited above.

Past FMR measurements on YIG single-crystal spheres and films for power levels above the linear regime have been complicated by sample heating effects, and it was necessary to perform the measurements under very low duty cycle conditions to avoid such effects.[4–7] In these previous works, measurements of the FMR profiles were made by sweeping the static field and monitoring the absorbed microwave power. The shifts in resonance position which occurred due to heating, caused by the associated changes in magnetization, anisotropy, and damping, led to complicated foldover effects. The low duty cycle approach eliminated these thermal effects and made it possible to determine the second-order threshold h_{crit} values at FMR with reasonable accuracy. The measurements here were obtained quite differently, by

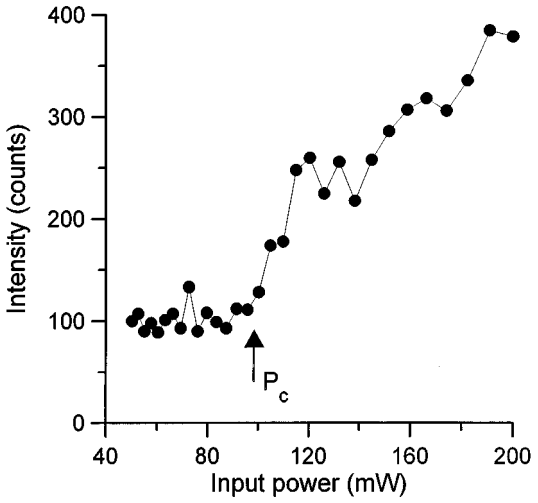

FIG. 3. Measured scattered light intensity for magnons as a function of the input microwave power level at a nominal pump frequency of 8.6 GHz. The arrow labeled P_c designates the critical power for the observed abrupt increase in the scattered light intensity. The data are for the 4.15-μm-thick YIG film with the static and linearly polarized microwave fields both in the plane of the film and mutually perpendicular, with a static field of 2338 Oe. The lines connecting the data points are intended to serve as a guide to the eye only.

(1) keeping the static field fixed and (2) directly observing the light scattering signal from the pumped magnons. Here, any heating effects which do occur would correspond to the steady state. Such considerations may be of importance for the second-order butterfly curve data to be presented in the next section. At very high powers, well above the spin-wave instability threshold, a severe degradation in the light scattering signals was found as well.

The threshold microwave power levels for second-order instability were determined versus the static magnetic field strength from light-scattering measurements. Both the magnons associated with FMR and the critical mode magnons generated through the second-order spin-wave instability processes occur at or close to the pump frequency ω_p. In order to detect the BLS signal associated with these magnons only, a gate pulse arrangement similar to one originally devised by Wilber *et al.*[25] was used to select out only that portion of the scattered light shifted from the laser frequency by ω_p. With the static magnetic field held constant, this scattered light signal was then measured as a function of the applied microwave pump power.

IV. RESULTS

Some representative results for the basic BLS versus microwave power measurement just outlined are shown in Fig. 3. The plot shows the measured scattered light photon count as a function of the input microwave power. These data are for a static magnetic field $H=2338$ Oe, somewhat above the FMR peak position at 2300 Oe. Recall that with the cavity, the nominal FMR frequency is shifted to about 8.6 GHz. The angle selective diaphragm was not in place for these measurements. Keep in mind that the detected photons correspond to BLS frequency shifts close to ω_p only. The vertical axis therefore represents (1) the residual low k magnon signal associated with the FMR response and (2) any low k contribution to the response associated with parametric magnons generated through the second-order processes. Also keep in mind that the actual FMR magnons at or near $k=0$ and the high k magnons in the $k=10^5$–10^6 rad/cm range are excluded by the scattering geometry.

Viewed in the context of the above remarks, the data in Fig. 3 are extremely interesting. The scattering signal is relatively constant at low power, and increases sharply but steadily above some critical input power. This critical threshold power is indicated as P_c in Fig. 3. The low power response represents a background count. If this response was due to FMR magnons, one would expect the signal level to increase with power input. A background response rather than a FMR response is reasonable, since $k\approx 0$ magnons are excluded by the scattering geometry.

It would be reasonable, as well, to associate the distinct increase in signal above the threshold P_c with the onset of nonlinear processes and parametric magnons excited through the Suhl second-order processes. Note, however, that the observed magnon signal cannot correspond to the high k magnons predicted from the Suhl theory. It appears, therefore, that one either has (1) additional low k magnons in addition to the expected high k critical mode magnons, or (2) critical mode low k magnons rather than the high k critical mode magnons predicted from bulk theory. Both options will be examined in more detail in the next section.

When the input power was increased further, beyond the range shown in Fig. 3, the light-scattering signal level was found to drop and exhibit transient effects one would expect from sample heating. That is, the response to an abrupt increase in power yielded a somewhat slower magnon response. These drops in signal intensity and transient responses were attributed to heating effects. These effects occurred only at power levels well above the P_c values associated with the onset of nonlinear processes.

Data similar to the results in Fig. 3 were obtained for a range of static fields from about 100 Oe below FMR to about 160 Oe above FMR. For fields further away from FMR, the threshold powers became too high to measure. These P_c versus H data were then used to construct a butterfly curve in the same spirit as the butterfly curves introduced above for parallel pumping and subsidiary absorption. In previous work, resonance saturation threshold power determinations have been typically limited to *one point* in field, namely, the FMR field. By extending these determinations to fields well below and well above the FMR field position, it has been possible to construct a second-order resonance saturation butterfly curve.

The minimum value of P_c was found to occur at the FMR field. This is reasonable, since the uniform mode response is largest at this point and the coupling between the uniform mode and the degenerate spin waves is the largest as well. This minimum P_c value was typically in the 10 mW range of input powers. This minimum threshold power will be denoted as $P_{c\text{-min}}$. The conventional butterfly curve plot is one of the microwave threshold field amplitude at the position of the sample, h_{crit} rather than some related input system power threshold such as P_c versus the static field H. For

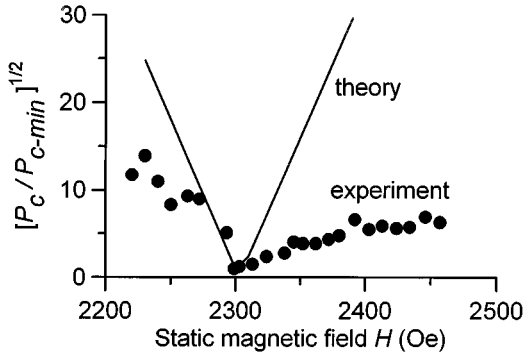

FIG. 4. Scaled resonance saturation butterfly curve plot of reduced threshold microwave field amplitude, shown in terms of critical powers P_c and $P_{c\text{-min}}$ as $[P_c/P_{c\text{-min}}]^{1/2}$, versus the in-plane static field H for the 4.15-μm-thick YIG film with the linearly polarized microwave field also in plane. The solid circles give the results of the measurements. The solid lines give the theoretical result based on the Suhl theory for bulk materials, the thin-film uniform mode response, and a fixed wave vector independent spin-wave linewidth. The nominal frequency for the data and the frequency for the theory was 8.6 GHz.

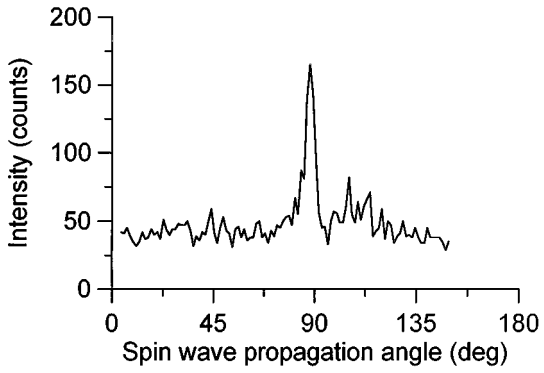

FIG. 5. Measurements of the BLS scattering signal as a function of the angle selective diaphragm slit angle position relative to the static field direction for the 4.15-μm-thick YIG film. The nominal frequency was 8.6 GHz and the static in-plane field was above resonance at about 2340 Oe, close to the value for Fig. 3. The input power was about 180 mW, well above the threshold power level in Fig. 3.

the present purposes, scaled butterfly curves were obtained in the form of plots of $[P_c/P_{c\text{-min}}]^{1/2}$ as a function of H.

A representative resonance saturation butterfly curve result is shown in Fig. 4. The plot shows values of $[P_c/P_{c\text{-min}}]^{1/2}$ as a function of the static field H. The data are shown by the solid circles. The solid line indicates a theoretical result based on the Suhl theory, a uniform FMR response, and a constant spin-wave linewidth. The theoretical result will be considered in the next section. Recall that the amplitude of a linearly polarized microwave field scales with the input power to the waveguide structure, so that $[P_c/P_{c\text{-min}}]^{1/2}$ represents the threshold microwave field amplitude normalized to the minimum threshold at FMR.

The reader familiar with parallel pump or subsidiary absorption butterfly curves will note the generally familiar appearance of the experimental results in Fig. 4. The data points show a minimum threshold position which increases as one moves either up or down in field. In the case of parallel pumping or subsidiary absorption, the minimum corresponds to the coincidence of some minimum threshold mode at $k=0$ with $\omega_p/2$. Here, the minimum corresponds to coincidence of the FMR frequency with spin waves at ω_p.

It is interesting to note that the increase in threshold as one moves up or down in field from the FMR position is: (1) not symmetric, and (2) not as sharp as one might expect from the narrow FMR response in Fig. 1. The solid line in Fig. 4 shows the increase one would expect based on the FMR response. The asymmetric character of the experimental results may be connected to heating effects and foldover considerations. The weaker than expected increase may be related to cavity loading effects. These considerations and their effect on the data will be discussed in more detail in the next section.

Additional measurements were made to further define the nature of the magnon signal responsible for the results in Figs. 3 and 4. For these measurements, the angle selective diaphragm was in place, as shown in Fig. 2, and data on the scattering signal intensity as a function of angle were obtained. Representative data are shown in Fig. 5. The static field for the measurements in Fig. 5 was set above resonance, at about 2340 Oe, close to the conditions represented in Fig. 3. The input power, on the scale of Fig. 3, was about 180 mW, well above threshold. Keep in mind that the slit diaphragm selects out only propagation angle and the signal still contains the full range of k values, $100 \leqslant k \leqslant 3.8\times10^4$ rad/cm. Also keep in mind that the angle parameter in Fig. 5 corresponds to the in-plane **k** direction, relative to the direction of the magnetic field **H**, for the magnons which are giving rise to the scattering signal.

The results in Fig. 5 are representative. Similar results were obtained for field values slightly below the FMR field. The key result is readily apparent from the well defined peak in the scattering signal. The peak is sharp, narrow, and symmetric. It appears to indicate the presence of a magnon mode with a well defined propagation angle centered at 85°–90°. The width of the peak is approximately 5°–10°.

These data provide two additional items of information concerning the critical modes. First, the nonlinear light-scattering signal observed in these measurements is not simply due to some residual nonlinear FMR response effect. If it were, there is no reason to expect one particular angle over another. Second, the signals observed here represent low k magnons associated with the parametric process and with a very well defined in-plane propagation direction of about 90° relative to the static field direction. As already indicated, such a low wave number critical mode component is not expected from the bulk theory. Moreover, the high k critical modes which *are expected* have a predicted propagation angle of 0°. It has already been emphasized that the discovery of low k modes does not exclude the presence of high k critical modes as well. Such modes, if present, are simply out of range for direct detection by the BLS technique in the forward scattering arrangement.

V. DISCUSSION

The essential results from the bulk spin-wave instability theory developed by Suhl and Schlömann were summarized

in Sec. II. Practical working equations for various sample shapes and pumping configurations for first-order processes have been developed by Patton.[23] The first-order theory has been extended by Wiese and co-workers[13] to include the effect of coupled modes close to the nominal parametric mode frequency at $\omega_k = \omega_p/2$.

There has been no similar development for second-order processes. Up to now, considerations of second-order processes have been limited to samples biased at FMR and working equations based on the bulk theory. Some working equations for thin-film FMR are given by Zhang *et al.*[6] The data in Fig. 4, as already indicated, represent a new perspective on resonance saturation in which one considers the threshold microwave field or power as a function of the static field and not just at the one field which corresponds to FMR. Working equations for such second-order FMR saturation butterfly curves may be obtained from a straightforward but tedious extension of the formalism in the references already cited. Such equations are summarized in the appendix. The essential result is an expression for the linearly polarized microwave field amplitude $h_c^{(2)}(\theta_k, \phi_k)$ at which a particular bulk spin wave at a frequency $\omega_k = \omega_p$ and propagation direction defined by polar and azimuthal spin-wave propagation angles θ_k and ϕ_k will be parametrically excited. The actual threshold microwave field amplitude for the spin-wave instability effect seen experimentally then corresponds to the minimum value of $h_c^{(2)}(\theta_k, \phi_k)$ over the range of available θ_k values at $\omega_k = \omega_p$ for the particular magnetic field of interest and the full range of ϕ_k values from zero to 2π. In line with the nomenclature of Refs. 6 and 23, this operational threshold microwave field amplitude will be designated as $h_{\text{crit}}^{(2)}$. Keep in mind that $h_{\text{crit}}^{(2)}$ will be a function of the static field H. Also keep in mind that each value of $h_{\text{crit}}^{(2)}$ carries with it a specific value of θ_k and of the corresponding wave number k for the minimum threshold critical mode. Let these critical mode parameters be denoted as $\theta_{k\text{-min}}$ and k_{min}, respectively.

The solid line in Fig. 4 represents the prediction from the bulk theory outlined above and the working equations given in the appendix. The vertical axis for the experiment corresponds to values of $[P_c/P_{c\text{-min}}]^{1/2}$ extracted from the threshold data. The appropriate corresponding parameter from the theory is $h_{\text{crit}}^{(2)}/h_{\text{crit-min}}^{(2)}$, where $h_{\text{crit-min}}^{(2)}$ is the minimum value of $h_{\text{crit}}^{(2)}$ over the range of static fields for the calculations. This minimum threshold occurs, of course, at the FMR field where the uniform precession amplitude is the largest. The calculations were made with parameters applicable to YIG films with the static and linearly polarized microwave magnetic fields both in-plane. The spin-wave linewidth was taken as fixed and **k** independent. The FMR linewidth was set at 1.5 Oe from the low power data in Fig. 1.

The most striking feature of the solid curve in Fig. 4 is in the distinct ''V'' shape for the predicted second-order butterfly curve. If this second-order threshold butterfly curve is due only to the loss term in the FMR response, one would expect a very sharp cusplike response with the appearance of a flipped over FMR absorption curve. The V shape obtained from the theory is due to the fact that the total FMR response provides the coupling which drives the instability, not just the out-of-phase absorptive response which leads to the loss curve in Fig. 1. The calculated V response is also symmetric. This is due to the assumed uniform mode FMR response for the analysis.

It is also important to note the minimum threshold spin-wave parameters $\theta_{k\text{-min}}$ and k_{min} which are associated with the solid curve in Fig. 4. As already indicated in Sec. II, the bulk theory gives $\theta_{k\text{-min}} = 0°$. The corresponding values of k_{min} at $\omega_k = \omega_p$ are in the $3–4\times10^5$ rad/cm range.

It is clear that the bulk theory result shown by the solid line in Fig. 4 shows significant departures from the experimental results. The minimum threshold points match up, of course, because both the data and the theoretical results have been normalized to minimum threshold values at the FMR field position. Even on this normalized scale, however, the experimental thresholds increase much more slowly as one moves away from the FMR position than does the result from bulk theory. The experimental result also shows a very significant asymmetry. The rise for fields below resonance follows the bulk theory for a small range of fields, while on the high-field side the increase is much slower. The apparent match-up on the low-field side may be real or fortuitous. This point will be considered shortly.

Apart from the problems immediately apparent from the data and theory in Fig. 4, there are serious problems of interpretation as well. Recall the critical mode properties obtained from the BLS data. The data indicated strong scattering from magnons with low wave numbers in the $10^2–4\times10^4$ rad/cm range and a well defined propagation angle at $\theta_k = 80°–90°$ propagation angle. These experimental observations are at odds with the predictions from bulk theory, which give $\theta_{k\text{-min}} = 0°$ and k_{min} values in the $3–4\times10^5$ rad/cm range. It is to be emphasized that the data do not exclude critical modes in the predicted range. The data simply reveal a strong signal at much lower wave numbers and propagation angles 85°–90° away from those for the high k modes.

The poor match-up between the data and the theory in Fig. 4 may be due to several factors, some connected with the experiment and some with bulk theory. Consider first the experimental factors. The first such factor concerns the symmetry of the uniform mode. The absorption profile in Fig. 1 clearly demonstrates that the overall response is not symmetric at all. The additional region of absorption somewhat higher in field than the main FMR peak is related to magnetostatic modes and the nonuniform microwave excitation over the sample. This near-uniform mode response in Fig. 1 would be expected to reduce the instability threshold microwave field amplitude for some range of fields 20–40 Oe above the FMR point. The reduced thresholds shown in Fig. 4 for fields above the FMR point extend to much higher fields. One can conclude, therefore, that the nonuniform microwave excitation is probably not responsible for the asymmetry in the threshold data in Fig. 4.

The second experimental factor concerns the cw microwave excitation used to excite the FMR response in the first place. Much of the previous work cited above supports the conclusion that cw microwave excitation inevitably leads to foldover effects of one kind or another. These past works have shown that even a small amount of heating of the YIG

sample can result in significant shifts in the FMR position. For the in-plane static field geometry used here, such a shift would be to higher static fields. Nominal heating effects, therefore, even below those needed to affect threshold onset data of the sort shown in Fig. 3, could cause an upfield shift in the FMR position and lead to the type of asymmetry evident in Fig. 4. A detailed study of the threshold onset response as a function of duty cycle would be needed to pinpoint these effects.

The third experimental factor concerns the strong cavity loading effects at FMR. Recall that the FMR absorption curve shown in Fig. 1 was obtained with a waveguide short. The high power measurements required the use of a cavity instead of a short, in order to achieve the microwave field amplitudes needed to drive the sample above threshold. The effect of the sample on the cavity response, however, was significant and was especially pronounced at FMR. This means that the assumption of a constant factor relating the input microwave power and the square of the microwave field amplitude at the sample position is only approximate. The threshold values in Fig. 4 are normalized to the values at resonance. The severe loading of the cavity at FMR means that the actual threshold microwave field amplitudes away from resonance would be larger than indicated by the data points in Fig. 4. On the scale of Fig. 4, a variable calibration would tend to produce an improved match with the theory. As with the previous point, a more quantitative discussion would require a detailed calibration of the microwave field versus input power for the loaded cavity *or* measurements in the shorted waveguide configuration with a much higher microwave power source than was available for the measurements.

Turn now to theoretical considerations. The solid line in Fig. 4 is based on the bulk theory as originally set forth in the Suhl and Schlömann references cited above. The thin-film geometry enters only in the uniform mode response analysis. This uniform mode was taken to be coupled to bulk spin-wave modes at $\omega_k = \omega_p$. None of the additional mode selection considerations for the thin-film geometry were considered. Work already cited by Wiese and co-workers for parallel pumping and subsidiary absorption has clearly shown that the standing wave nature of the spin-wave modes in thin films, both across the film thickness and across the lateral dimensions of the film, can significantly affect the critical modes and the butterfly curves for first-order processes. Similar effects are also to be expected for second-order processes. The inclusion of such modes in the second-order theory would be formidable. Such an analysis has not yet been done.

Related to the above is the possible dilemma concerning the observed critical mode component at low wave number and a propagation angle of 85°–90°, relative to the predictions from bulk theory of critical modes at high wave number and a propagation angle of 0°. The description of this situation as a *possible dilemma* is deliberate. As already emphasized, the data do not preclude the existence of a critical mode component at high k. Such modes are simply not accessible in the BLS forward scattering geometry. A thin-film specific theory which includes coupled spin-wave modes for the actual thin-film geometry, moreover, may well lead to predicted critical modes at k values and propagation angles which are significantly different from those predicted from the bulk theory.

With no such theory yet available, any quantitative discussion of these points is moot. However, several qualitative points based on the previous experience with first-order processes are worth observation. First, it is worthwhile to note that the k dependence of the spin-wave linewidth can have an important effect on the critical modes with the lowest threshold.[11,27,28] In the case of subsidiary absorption, this k dependence leads to rather drastic changes in the butterfly curve in the form of a kink effect and a discontinuous jump of the critical modes to much lower wave numbers and much higher propagation angles than one would expect if this dependence is ignored. The reader may consult Ref. 11 by Patton and Jantz or the review chapter by Chen and Patton[21] for a detailed discussion of these effects. Second, it is also important to note that the actual thin-film modes play a critical role in subsidiary absorption and lead to effects which can be similar to the effects of a **k**-dependent spin-wave linewidth.[13] It is entirely possible that a full second-order spin-wave instability analysis for the thin-film geometry will lead to predicted critical modes which are very different from those obtained from the bulk theory.

ACKNOWLEDGMENTS

Dr. Wiese was supported in part on a fellowship from Deutsche Forschungsgemeinschaft, Bonn, Germany. The YIG films were provided by Dr. J. D. Adam, Westinghouse Science and Technology Center, Pittsburgh, PA. The research was supported by the United States Office of Naval Research, Grant No. N00014-90-J-4078 and No. N00014-94-1-0096, the National Science Foundation, Grant No. DMR-8921761 and No. DMR-9400276, and the United States Army Research Office, Grants No. DAAL03-91-G-0327 and No. DAAH04-95-1-0325. Dr. M. A. Wittenauer is acknowledged for a critical reading of the manuscript.

APPENDIX

In the appendix to Ref. 6, working equations to obtain the threshold microwave field amplitudes for second-order spin-wave instability processes at ferromagnetic resonance were summarized for different pumping configurations in a thin magnetic film. The purpose of this appendix is to provide similar working equations for static fields away from the field for ferromagnetic resonance. The notation and nomenclature follow the original formulation of the analysis for first-order processes in Ref. 23. The working equations obtained in Ref. 6 were specific to the case of a sample biased at ferromagnetic resonance and for critical modes at $\theta_k = 0$. The relatively simple final equations were approximate, based on the assumption that the anti-Larmor component of the FMR response was small and could be neglected. Here, with a view toward the numerical evaluation of the second-order threshold butterfly curve shown in Fig. 4, anti-Larmor terms in the response will not be neglected. The results will

be limited to the case of a linearly polarized microwave field applied perpendicular to the static field, and with both fields in the plane of the film.

The end result needed to evaluate the theoretical curves in Sec. IV is an expression for the linearly polarized microwave field amplitude, $h_c^{(2)}(\theta_k,\phi_k)$, at which a particular bulk spin wave at a frequency $\omega_k=\omega_p$ and propagation direction defined by θ_k and ϕ_k will be parametrically excited. As in Ref. 23 and the appendix to Ref. 6, this field is obtained by equating the coefficient for energy flow into a particular spin-wave mode, $G_k^{(2)}$, and the relaxation rate η_k for the decay of energy out of that mode. This relaxation rate is connected to the conventional spin-wave linewidth ΔH_k through the relation $\Delta H_k=2\eta_k/|\gamma|$, where γ denotes the gyromagnetic ratio. For YIG, $|\gamma|$ is 2.8 GHz/kOe. In Ref. 6, this coupling coefficient was given in the form

$$G_k^{(2)}=\left(\frac{|\gamma|\cdot h_0}{2}\right)^2\left(\frac{e^{2i\phi_k}}{4\omega_p}\right)W^{(2)}, \tag{A1}$$

where h_0 denotes the amplitude of the linearly polarized microwave field, ϕ_k is the azimuthal spin-wave propagation angle defined in the context of the sample orientation and microwave pumping geometry,[23] and $W^{(2)}$ is a reduced coupling factor with units of frequency. The condition $G_k^{(2)}=\eta_k$ will yield an expression for h_0 which corresponds to $h_c^{(2)}(\theta_k,\phi_k)$.

The reduced coupling factor $W^{(2)}$ may be written, as in Ref. 6, in terms of the basic magnetic parameters, the uniform mode response parameters, and the spin-wave parameters. From the full second-order instability analysis, this $W^{(2)}$ factor is given by

$$\begin{aligned}W^{(2)}=&(A_k+\omega_p)(\sigma q_L^2+q_L+\delta q_L q_A^*)e^{-2i\phi_k}+(A_k-\omega_p)\\&\times(\sigma q_A^{*2}+q_A^*+\delta^* q_L q_A^*)e^{2i\phi_k}-B_k[1/2(q_A^*+q_L)\\&+Rq_L q_A^*+S(q_L^2+q_A^{*2})].\end{aligned} \tag{A2}$$

The A_k and B_k parameters in Eq. (A2) are the same as those obtained from spin-wave theory

$$A_k=|\gamma|(H+Dk^2+2\pi M_s\sin^2\theta_k), \tag{A3}$$

$$B_k=|\gamma|2\pi M_s\sin^2\theta_k. \tag{A4}$$

In the above, H refers to the static in-plane field, D is the exchange stiffness parameter, and M_s denotes the saturation magnetization. For YIG, D is approximately 5.4×10^{-9} Oe cm^2/rad^2 and $4\pi M_s$ is 1750 G. Note that the spin-wave frequency is given by $\omega_k=[|A_k|^2-|B_k|^2]^{1/2}$. The second-order threshold condition $\omega_k=\omega_p$ establishes a constraint between k and θ_k which simplifies the minimization procedure which is ultimately done to determine the threshold microwave field amplitude $h_{\rm crit}^{(2)}$ for a given field H.

The σ, δ, R, and S parameters in Eq. (A2) are given by

$$\sigma=|\gamma|[Dk^2+2\pi M_s(2\cos^2\theta_k-1)], \tag{A5}$$

$$\delta=|\gamma|2\pi M_s(\sin^2\theta_k e^{2i\phi_k}+1), \tag{A6}$$

$$R=|\gamma|2\pi M_s(3\sin^2\theta_k-2), \tag{A7}$$

and

$$S=-|\gamma|\pi M_s. \tag{A8}$$

Equation (A5) for σ differs from the one introduced in Ref. 6. The difference is due to the fact that the Eq. (A5) applies for the in-plane magnetized film, and the σ parameter in Ref. 6 was for external static magnetic field perpendicular to the film surface. Unfortunately, the same σ was also used for the in-plane magnetized film case in Ref. 6. Because of this error, the $\omega_m=|\gamma|4\pi M_s$ factor in the square root term of Eqs. (3) and (4) of Ref. 6 should be replaced by $\omega_m/2$.

The q_L and q_A parameters are, as in Refs. 6 and 23, reduced expressions for the Larmor and anti-Larmor circularly polarized components of the uniform precession response

$$\begin{aligned}q_{L,A}=&\frac{i[|\gamma|(H+4\pi M_s)\pm\omega_p]}{T},\\T=&(|\gamma|H)[|\gamma|(H+4\pi M_s)]-\omega_p^2+i(|\gamma|\Delta H/2)\\&\times[|\gamma|(2H+4\pi M_s)].\end{aligned} \tag{A9}$$

The $\pm$ in the numerator term of Eq. (A9) refer to q_L and q_A, respectively. The ΔH parameter is the half power ferromagnetic resonance linewidth of the film.

From the equations specified above, one solves the equation $|G_k^{(2)}|=(|\gamma|\Delta H_k)/2$, in combination with Eq. (A1), for the microwave field amplitude h_0. This amplitude then corresponds to the threshold field $h_c^{(2)}(\theta_k,\phi_k)$ for a given spin wave at wave number k, polar and azimuthal spin-wave propagation angles θ_k and ϕ_k respectively, and frequency, $\omega_k=\omega_p$. As already indicated, k and θ_k are connected through the dispersion relation $\omega_k=[|A_k|^2-|B_k|^2]^{1/2}$ and the $\omega_k=\omega_p$ condition.

The minimization of $h_c^{(2)}(\theta_k,\phi_k)$ over the range of available θ_k values at a given value of the static field H and over the full range of ϕ_k values between zero and 2π yields the desired value of the instability threshold microwave field amplitude $h_{\rm crit}^{(2)}$. For fields above the FMR field, the range of available θ_k values is from some upper limit which is below 90° down to $\theta_k=0$. For fields above the FMR field, θ_k ranges over the full span of values within the spin-wave band from 90° at $k=0$ down to 0° at the maximum k value allowed at $\omega_k=\omega_p$. The actual procedure was carried out numerically to obtain the values of $h_{\rm crit}^{(2)}$ as a function of H needed to construct the solid curve in Fig. 4. For all fields in the range shown in Fig. 4, the minimum threshold occurred for a θ_k of zero and, of course, no dependence on ϕ_k.

[1] D. D. Stancil, *Theory of Magnetostatic Waves* (Springer, New York, 1993).

[2] P. Kabos, in *High Frequency Processes in Magnetic Materials*, edited by G. Srinivasan and A. N. Slavin (World Scientific, Singapore, 1995), Chap. 1.

[3] L. M. Silber, C. E. Patton, and H. F. Naqvi, J. Appl. Phys. **54**, 4071 (1983).

[4] K. D. McKinstry, C. E. Patton, and M. V. Kogekar, J. Appl. Phys. **58**, 925 (1985).

[5] Y. T. Zhang, C. E. Patton, and M. V. Kogekar, IEEE Trans. Magn. **22**, 993 (1986).

[6] Y. T. Zhang, C. E. Patton, and G. Srinivasan, J. Appl. Phys. **63**, 5433 (1988).

[7] M. Chen, C. E. Patton, G. Srinivasan, and Y. T. Zhang, IEEE Trans. Magn. **25**, 3485 (1989).

[8] P. Dorsey, J. B. Sokoloff, and C. Vittoria, J. Appl. Phys. **74**, 1938 (1993).
[9] See, for example, *Nonlinear Phenomena and Chaos in Magnetic Materials*, edited by P. E. Wigen (World Scientific, Singapore, 1994).
[10] G. Wiese, Z. Phys. B **91**, 57 (1993).
[11] C. E. Patton and W. Jantz, J. Appl. Phys. **50**, 7082 (1979).
[12] G. Wiese, P. Kabos, and C. E. Patton, J. Appl. Phys. **74**, 1218 (1993).
[13] G. Wiese, P. Kabos, and C. E. Patton, Phys. Rev. B **51**, 15085 (1995).
[14] W. Wettling, W. D. Wilber, P. Kabos, and C. E. Patton, Phys. Rev. Lett. **51***/*, 1680 (1983).
[15] W. D. Wilber, J. G. Booth, C. E. Patton, G. Srinivasan, and R. W. Cross, J. Appl. Phys. **64**, 5477 (1988).
[16] P. Kabos, G. Wiese, and C. E. Patton, Phys. Rev. Lett. **72**, 2093 (1994).
[17] G. Srinivasan, C. E. Patton, and J. G. Booth, J. Appl. Phys. **63**, 3344 (1988).
[18] H. Suhl, J. Phys. Chem. Solids **1**, 209 (1957).
[19] E. Schlömann, Technical Report No. R-48, Raytheon Company, Research Division, 1959, (unpublished).
[20] C. E. Patton, in *Magnetic Oxides*, Part 2, edited by D. J. Craik (Wiley, London, 1975), Chap. 10.
[21] M. Chen and C. E. Patton, in Ref. 9, Chap. 3.
[22] E. Schlömann, J. J. Green, and U. Milano, J. Appl. Phys. **31**, 3865 (1960).
[23] C. E. Patton, J. Appl. Phys. **40**, 2837 (1969).
[24] C. E. Patton and J. J. Green, IEEE Trans. Magn. **5**, 626 (1969).
[25] W. D. Wilber, W. Wettling, P. Kabos, C. E. Patton, and W. Jantz, J. Appl. Phys. **55**, 2533 (1984).
[26] Interferometer system manufactured by JRS Ltd., Zwillikerstrasse 8, 8910 Affoltern a. A., Switzerland.